RSC Advances

PAPER

View Article Online
View Journal | View Issue

Cite this: *RSC Adv.*, 2015, **5**, 27759

Electrochemical response of nitrite and nitric oxide on graphene oxide nanoparticles doped with Prussian blue (PB) and Fe_2O_3 nanoparticles

Abolanle S. Adekunle,*[ab] Seonyane Lebogang,[a] Portia L. Gwala,[a] Tebogo P. Tsele,[a] Lukman O. Olasunkanmi,[ab] Fayemi O. Esther,[a] Diseko Boikanyo,[a] Ntsoaki Mphuthi,[a] John A. O. Oyekunle,[b] Aderemi O. Ogunfowokan[b] and Eno E. Ebenso*[a]

Electrocatalytic behaviour of graphene oxide (GO), iron(III) oxide (Fe_2O_3) and Prussian blue (PB) nanoparticles and their nanocomposite towards nitrite (NO_2^-) and nitric oxide (NO) oxidation in neutral and acidic media respectively was investigated on a platinum (Pt) modified electrode. Successful synthesis of these nano materials was confirmed using microscopic and spectroscopic techniques. Successful modification of the electrode was confirmed using cyclic voltammetry (CV) and electrochemical impedance spectroscopy (EIS). The results showed that the Pt–GO–Fe_2O_3 and Pt–GO–PB nanocomposite modified electrodes gave a faster electron transfer process in both a 5 mM Ferri/Ferro ($[Fe(CN)_6]^{3-/4-}$) redox probe and 0.1 M phosphate buffer solution (PBS). The Pt–GO–Fe_2O_3 and Pt–GO–PB electrodes also gave an enhanced NO_2^- and NO oxidation current compared with bare Pt and the other electrodes studied. Electrocatalytic oxidation of the analyte occurred through a simple diffusion process but were characterized with some level of adsorption. Tafel slopes *b* of 468.4, 305.2 mV dec^{-1} (NO_2^-, NO); and 311.5, 277.2 mV dec^{-1} (NO_2^-, NO) were obtained for the analyte at the Pt–GO–Fe_2O_3 and Pt–GO–PB electrode respectively. The Pt–GO–Fe_2O_3 limit of detection and sensitivity in NO_2^- and NO are 6.60 μM (0.0084 μA μM^{-1}) and 13.04 μM (0.0160 μA μM^{-1}) respectively, while those of the Pt–GO–PB electrode are 16.58 μM (0.0093 μA μM^{-1}) and 16.50 μM (0.0091 μA μM^{-1}). The LoD compared favourably with literature reported values. Pt–GO–Fe_2O_3 gave a better performance to NO_2^- and NO electrooxidation, good resistance to electrode fouling, a higher catalytic rate constant and lower limit of detection. The adsorption equilibrium constant β and the standard free energy change ΔG^0 due to adsorption are 10.29×10^3 M^{-1} (−22.89 kJ mol^{-1}) and 3.26×10^3 M^{-1} (−20.04 kJ mol^{-1}) for nitrite and nitric oxide respectively at the Pt–GO–Fe_2O_3 electrode. An interference study has also been reported. The fabricated sensors are easy to prepare, cost effective and can be applied for real sample analysis of nitrite and nitric oxide in food, water, biological and environmental samples.

Received 5th February 2015
Accepted 11th March 2015

DOI: 10.1039/c5ra02008e

www.rsc.org/advances

1. Introduction

It is well known that bulk materials based on TiO_2, SiO_2, aluminium and iron oxides have been massively produced for many years. Recently, nanoparticulate versions of these metal oxides have been manufactured.[1] They are introduced in commercial products such as cosmetics and sunscreens (TiO_2, Fe_2O_3 and ZnO),[1] fillers in dental fillings (SiO_2),[2] as catalysts (TiO_2, Fe_2O_3),[3–5] and as fuel additives (CeO_2).[6] Iron oxide nanoparticles have attracted tremendous applications in the areas of nanotechnology and electrochemical sensors recently because of their interesting electron transport behaviour and excellent catalytic properties.[4–8] Magnetite (Fe_3O_4), maghemite (γ-Fe_2O_3), and hematite (α-Fe_2O_3) are probably the most common of the many oxide forms in which iron oxides exist in nature.[9] Prussian blue (PB) is an iron cyanide complex (Fe_4(III)$[Fe$(II)$(CN)_6]_3$), used as an electron-transfer mediator due to its excellent electrocatalytic properties. It has found applications in ion selective electrodes,[10] charge storage devices,[10] catalysis,[11] and biosensors.[12] PB modified electrodes exhibit a significantly decreased background current, resulting in improved signal-to-noise ratio. Graphene based materials is recently gaining serious attention because of their potential in designing electronics, sensing, and energy conversion devices.[13–17] Graphene oxide (GO) is obtained from chemical oxidation of graphite flakes to obtain an exfoliated two dimensional carbon sheets with excellent properties at nanoscale level.[18,19] The exact structure of GO is difficult to

[a]*Material Science Innovation and Modelling (MaSIM) Research Focus Area, Faculty of Agriculture, Science and Technology, North-West University (Mafikeng Campus), Private Bag X2046, Mmabatho 2735, South Africa. E-mail: Eno.Ebenso@nwu.ac.za; sadekpreto@gmail.com; Fax: +27 183892052; Tel: +27 183892050; +27 183892051*

[b]*Department of Chemistry, Obafemi Awolowo University, Ile-Ife, Nigeria*

determine, but has been attributed to the interruption of the aromatic lattice of graphene by epoxides, alcohols, ketone carbonyls, and carboxylic groups.[20,21]

Fe_2O_3 and GO–Fe_2O_3 modified electrodes have previously been used for the detection of many analytes including nitrite,[7] dopamine,[22] folic acid,[23] hydrogen peroxide[24] and ammonia.[25] Similarly PB and GO–PB modified electrodes have also been used for the detection of many molecules including hydrogen peroxide,[26] glucose,[27] and α2,6-sialylated glycans in human serum.[28] However, the extent and the mechanism for the electron transport of the GO–Fe_2O_3 modified electrodes are not clearly understood. Electron transport (ET) process between the surface active material and the underlying electrode is important in achieving a maximal overlap between electrode modifier, the electrolyte or the analyte in solution for enhanced or active electrocatalysis.

Nitrite (NO_2^-) is an important environmental molecule which is found in the natural environment and food because of its application as food preservative.[29] Thus it has gained research interest in both biological and environmental studies because of its health implications.[29–38] The nitrite ion combines with blood pigments to produce *meta*-haemoglobin which causes oxygen depletion to the tissues.[39] It also forms highly carcinogenic *N*-nitrosamine compounds when combined with amines and amides in the stomach.[39] Therefore, quantitative determination of nitrite in drinking water to access its quality, wastewater treatment, in food and for the control of remediation procedures cannot be overemphasized. Nitric oxide (NO) on the other hand is a free radical and thus highly reactive toward molecular oxygen, peroxides, radicals, and metals, including metal centers such as hemoglobin.[40,41] It is also a small and electrically neutral molecule in physiological buffer which enables NO to permeate biological membranes and diffuse quickly.[42] Thus, there is need for the detection and quantification of nitrite and nitric oxide using simple, effective and less expensive analytical techniques. Several methods have been developed for nitrite determination including spectrophotometry,[43] chemiluminescence,[44] chromatography,[45] capillary electrophoresis,[46] titrimetric[47] and electrochemical methods[7,29,31] but with one drawback or the other. Many of these procedures are time-consuming, but the electrochemical technique has been identified to provide cheaper, faster and real-time analysis.

In this work, Fe_2O_3 and Prussian blue (Fe_4(III)[Fe(II) $(CN)_6]_3$) nanoparticles were investigated to study their electrocatalytic behaviour towards nitrite (NO_2^-) and nitric oxide (NO) oxidation on graphene oxide platinum modified electrode. Electrocatalytic oxidation of the analytes was successful on the modified electrode but characterized by adsorption process probably due to the porous GO support and strong binding of the analytes on the electrode. Pt–GO–Fe_2O_3 modified electrode proved to be the best electrode in terms of NO_2^- and NO oxidation current, resistance to electrode poisoning and limit of detection of the analytes. The sensor is easy to fabricate, cost effective and could be used for routine determination of nitrite and nitric oxide in food and environmental matrices. Interference study has also been carried out.

2. Experimental

2.1. Materials and reagents

Platinum electrode (2 mm diameter) was purchased from CH Instrument USA. Chemicals and reagents used were of analytical grade and obtained from Sigma-Aldrich chemicals, Merck chemicals and LabChem. They include, graphite flakes, sodium nitrate ($NaNO_3$), sulphuric acid (H_2SO_4), potassium permanganate ($KMnO_4$), hydrochloric acid (HCl), hydrogen peroxide (H_2O_2), sodium nitrite ($NaNO_2$), $FeCl_3 \cdot 6H_2O$, $K_4[Fe(CN)_6]$, KCl, disodium hydrogen phosphate ($Na_2HPO_4 \cdot 2H_2O$), sodium dihydrogen phosphate ($NaH_2PO_4 \cdot 2H_2O$), phosphoric acid (H_3PO_4) and dimethylformamide (DMF). Ultra pure water of resistivity 18.2 MΩ was obtained from a Milli-Q Water System (Millipore Corp., Bedford, MA, USA) and was used throughout for the preparation of solutions. A phosphate buffer solution (PBS) of pH 3.0 and 7.0 was prepared with appropriate amounts of $NaH_2PO_4 \cdot 2H_2O$, $Na_2HPO_4 \cdot 2H_2O$, and H_3PO_4, and adjusted with 0.1 M H_3PO_4 or NaOH. Prepared solutions were purged with pure nitrogen to eliminate oxygen and prevent any form of external oxidation during the electrochemical experiments.

2.1.1 Synthesis of iron oxide (Fe_2O_3) and the Prussian blue (PB) nanoparticles. The synthesis route for the Fe_2O_3 nanoparticles has already been described and reported in previous work.[4] The PB nanoparticles was synthesized by simply mixing and stirring together 50 mL each of 10^{-2} M $K_4[Fe(CN)_6] \cdot 6H_2O$ and 10^{-2} M $FeCl_3 \cdot 6H_2O$ for 24 h. The resulting powder was filtered, washed with distilled-deionised water and dried. The synthesized Fe_2O_3 and PB powder were characterized using different spectroscopic and microscopic techniques.

2.1.2 Synthesis of graphene oxide (GO). Graphene oxide was synthesized from oxidation of graphite using Hummer's method.[18,48] 2.5 g graphite flakes and 1.25 g $NaNO_3$ were mixed with 60 mL H_2SO_4 in 250 mL flask and stirred for 30 minutes in an ice bath, 7.5 g $KMnO_4$ was added slowly to the suspension while maintaining reaction temperature lower than 20 °C. The reaction mixture was left overnight at room temperature. 75 mL of deionised water was added and stirred at 98 °C for a day. After the addition of 25 mL H_2O_2 (30%), the mixture was then washed with 5% HCl and water. The solution was filtered, dried in the oven at 60 °C and the graphene oxide was obtained as a gray powder.

2.2. Equipment and procedure

The Transmission electron microscopy (TEM) experiment was performed using a Tecnai G2 Spirit FEI (USA). FTIR and UV-vis experiments were carried out using Fourier Transform Infrared spectrophotometer (Agilent Technology, Cary 600 series FTIR spectrometer, USA) and UV-visible spectrophotometer (Agilent Technology, Cary series UV-vis spectrometer, USA), while the Raman spectra were obtained using Xplora Horiba Raman Spectrometer (Olympus BX41 microscope, UK). Electrochemical experiments were carried out using an Autolab Potentiostat PGSTAT 302 (Eco Chemie, Utrecht, and The Netherlands) driven by the GPES software version 4.9. Electrochemical impedance spectroscopy (EIS) measurements were performed with Autolab

Frequency Response Analyser (FRA) software between 10 kHz and 1 Hz using a 5 mV rms sinusoidal modulation with the solution of the analyte at their respective peak potential of oxidation (*vs.* Ag|AgCl in sat'd KCl). A Ag|AgCl in saturated KCl and platinum wire were used as reference and counter electrodes respectively. A bench top Crison pH meter, Basic 20+ model, was used for pH measurements. All experiments were performed at 25 ± 1 °C while the solutions were de-aerated before every electrochemical experiment.

2.3. Electrode modification procedure

Electrode modification was investigated using the drop-dry method. Firstly, the platinum electrode was cleaned by gentle polishing in aqueous slurry of alumina nanopowder (Sigma-Aldrich) on a SiC-emery paper followed by a mirror finish on a Buehler felt pad. The electrode was later subjected to ultrasonic vibration in water, and then absolute ethanol to remove residual alumina particles that are trapped on the surface. 10 μL drops of the prepared nanocomposite (5 mg each of GO and Fe_2O_3 in 1 mL DMF) was dropped on the bare Pt and dried in an oven at 50 °C for 2 min to obtain Pt–GO–Fe_2O_3. Similar procedure was used to obtain Pt–GO–PB modified electrodes. Other electrodes prepared by the drop-dry method are Pt–GO, Pt–Fe_2O_3 and Pt–PB.

3. Results and discussions

3.1. FTIR, Raman, UV-vis, XRD and TEM characterization

The FTIR spectra of the graphite flake (G) and the synthesized graphene oxide (GO) are shown in Fig. 1. The FTIR spectrum of G showed characteristic peaks at absorption bands 2164, 2402 and 2737 cm^{-1} respectively with a sharp peak at 2164 cm^{-1}. However on modification to GO, the peak at 2164 cm^{-1} disappeared while the peak at 2737 cm^{-1} shifted to lower absorption band (2654 cm^{-1}). Some new peaks emerged at 1589, 1646, 1797, 1722, 2084, 2283, 3733 and 33 776 cm^{-1} respectively, with sharp absorption bands at 3733 and 33 776 cm^{-1} and another at 1646 attributed to O–H groups stretching and bending vibrations of adsorbed water molecules[49] suggesting successful modification of G to GO. The absorption band at 1646, 1797 and 1722 cm^{-1} could be due to stretching vibration of the C=C and the C=O of the carboxylic acid and carbonyl groups present at the edges of the GO.[49,50] The presence of these oxygen-containing groups reveals that the graphite has been oxidized.

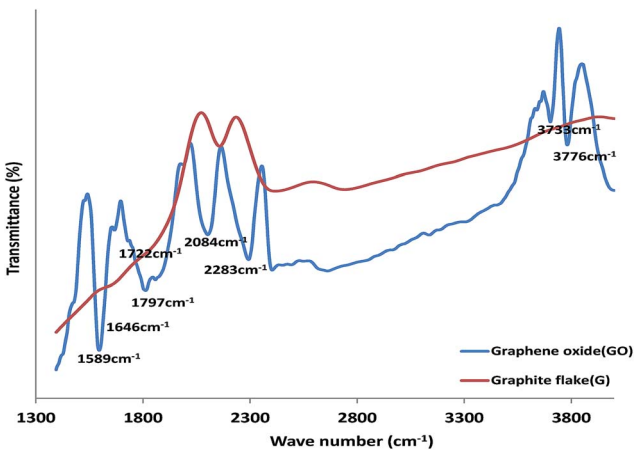

Fig. 1 (a) Comparative FTIR spectra of graphite flake (G) and graphene oxide (GO).

The Raman spectra of crystalline graphite flake (G) (Fig. 2a) show characteristic sharp band at 1583 cm^{-1} which has constantly been reported in literature.[51,52] Additional bands observed at 2334 and 2502 cm^{-1} are second order features. These second order bands have been attributed to overtones of Raman forbidden fundamentals.[52] The Raman spectra of graphite oxide (GO) (Fig. 2b) show the characteristic bands at 1340 and 1585 cm^{-1} respectively. These bands compare favourably with reports in literature[53–55] and show a blue shift in the G-band from G to GO (1583 *vs.* 1586 cm^{-1}) which confirm successful formation of GO. Successful formation of Fe_2O_3 was also confirmed from the Raman spectra in Fig. 2c in which some bands characteristic of Fe_2O_3 were observed.

The Raman spectra of Prussian blue (PB) presented in Fig. 2d show a band at 2139 cm^{-1} attributed to the stretching vibration of C–N triple bond in PB. Appearance of other bands along side C–N stretching frequency have also been reported[56] and attributed to co-precipitation of ferricyanide ion. The Raman spectra for GO–Fe_2O_3 (Fig. 2e) and GO–PB composite mixture (Fig. 2f) show the characteristic bands observed in both pure GO, Fe_2O_3 and PB in the composite. A slight shift in the G-band of GO to 1575 cm^{-1} in both composite was observed indicating the formation of the GO–Fe_2O_3 and GO–PB composite.

Fig. 3 is the UV-vis spectra of GO, GO–Fe_2O_3 and GO–PB respectively. The GO has characteristic absorption peaks at 219 and 250 nm. The peak at 250 nm has been reported at 237 nm,[57] and 230 nm (ref. 58) by other authors, and was described as the π–π* transition of the atomic C–C bonds of GO. GO–Fe_2O_3 spectrum showed reduction in GO peaks and appearance of a new peak at 282 nm confirming formation of GO–Fe_2O_3 nanocomposite through ionic interactions. The GO–PB UV-vis spectrum showed decrease in the GO peak intensity and an appearance of a new peak at approximately 700 nm (inset in Fig. 3), corresponding to the mixed-valence charge-transfer absorbance of the [Fe(II)–C–NFe(III)] complex. This new peak along with the GO peak confirms successful formation of GO–PB nanocomposite. The PB forms a stable nano films with the GO through both π–π and electrovalent interactions.

The XRD profile of the Fe_2O_3 nanoparticles has been reported in previous study.[4] XRD profile of the Fe_2O_3 nanoparticles is characterized with peaks at 2θ, 21.3, 35.2, 41.5, 50.6, 62.6, 67.4 and 74.3, which are indexed as (111), (220), (311), (400), (422) and confirmed the cubic spinel structure for γ-Fe_2O_3.[4] The estimated crystal size from the peaks is 10.3 nm.[4] The XRD profile of the PB nanoparticles (Fig. 4) was characterized with peaks at 2θ = 17.9, 25.1, 29.1, 30.4, 35.6, 40.1, 43.9, 46.6, 50.6, 54.6, 57.6, 60.1, 68.9, 70.8, 74.3, and 77.0, corresponding to Miller indices (200), (220), (311), (400), (420), (422), (440), (622), (642) and (800) indicating a cubic crystal structure for the PB

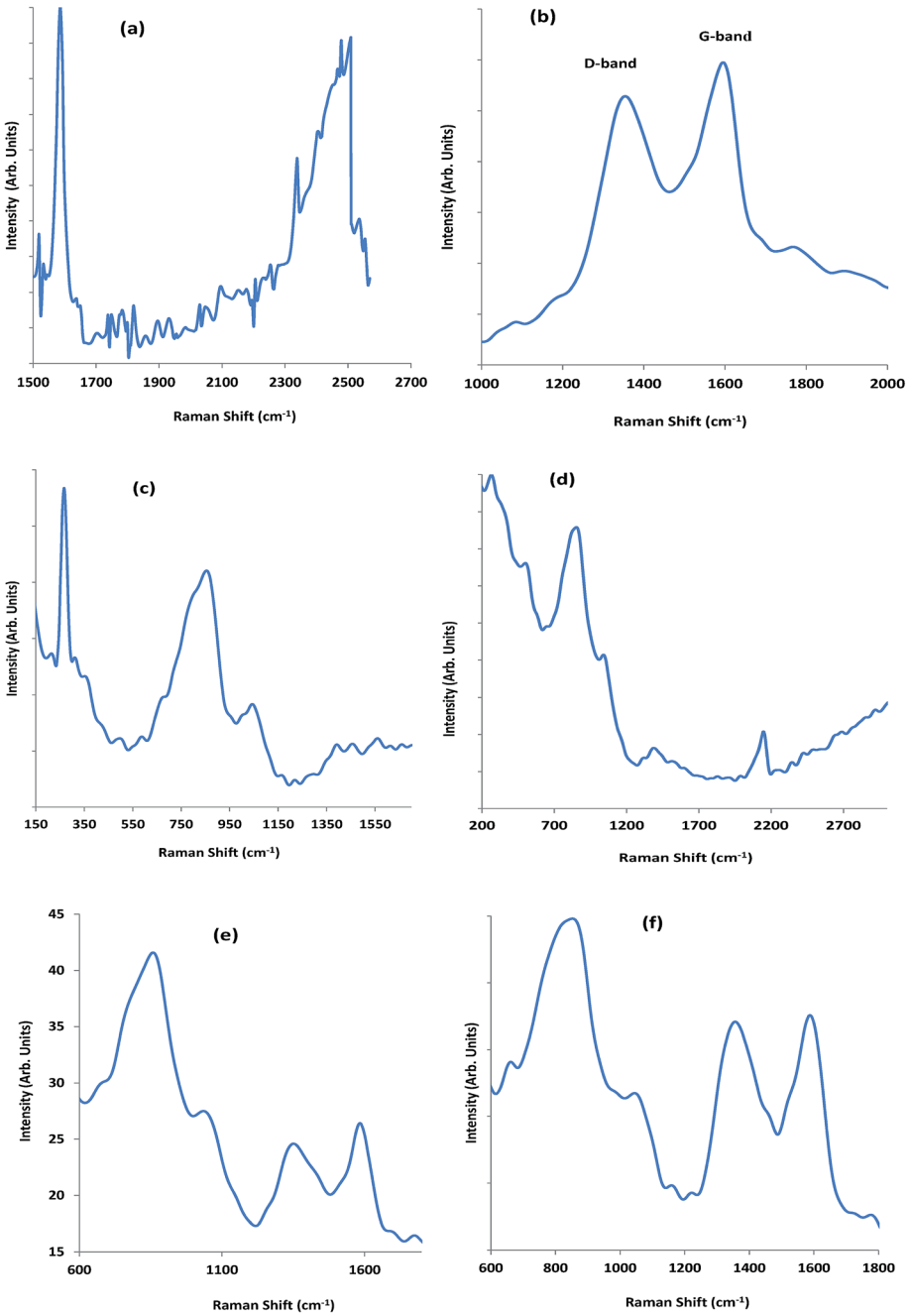

Fig. 2 Raman spectra of (a) graphite flake G (b) graphene oxide GO (c) Fe_2O_3 nanoparticles (d) PB nanoparticles (e) GO–Fe_2O_3 and (f) GO–PB.

nanoparticles. Using Debye–Scherrer formula,[53] the average crystal size of the PB particles was estimated to be 15 nm.

Fig. 5 is the TEM images of Fe_2O_3 nanoparticles (Fig. 5a) and PB nanoparticles (Fig. 5b). The TEM images show that the Fe_2O_3 particles appeared crystalline and evenly distributed; while the PB nanoparticles appeared more crystalline in nature, forming aggregated particles and PB nanoplatelets probably due to CN functional groups with electron reach nitrogen centre influencing intermolecular interactions between the PB particles through either strong π–π bonding or electrostatic linkage. The average particle size for Fe_2O_3 and PB vary from 5–20 nm and 2–30 nm respectively. Compared with PB and Fe_2O_3 alone, the TEM pictures of GO–Fe_2O_3 (Fig. 5c) appeared more crystalline while GO–PB appeared more porous (Fig. 5d). Both Fe_2O_3 and PB nanoparticles formed an aggregated particles around GO probably due to strong ionic interaction between these nanoparticles and oxygen rich GO. The average particle size distribution of the nanocomposite from the TEM image was estimated to be 15–30 nm. The reported particle sizes were obtained after calibrating the scale of the TEM image using the UTHSCSA Image Tool for windows version 3.0. The particle size 5–20 nm for Fe_2O_3 agreed closely with 8.6 nm for γ-Fe_2O_3 nanoparticles[59] and 10 nm for α-Fe_2O_3 made by microwave synthesis[60] but less than 100 nm reported Fe_2O_3 prepared by hydrothermal method.[7]

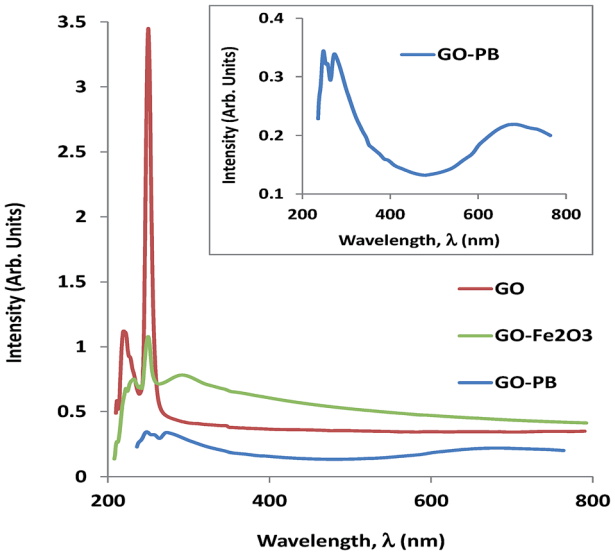

Fig. 3 UV-vis spectra of graphene oxide (GO), GO–Fe_2O_3 and GO–PB.

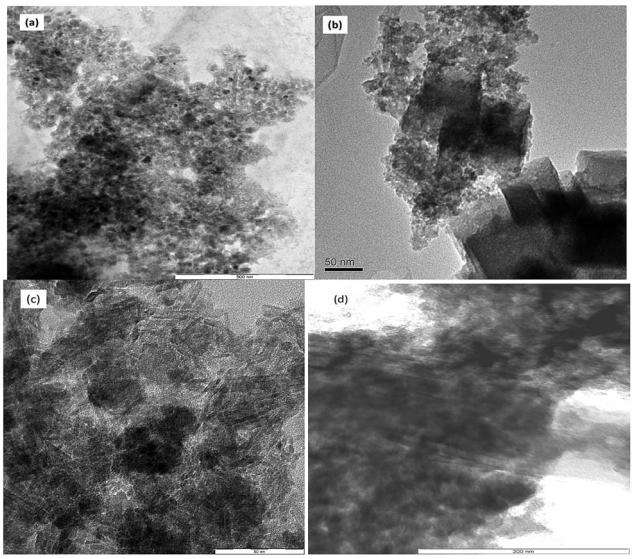

Fig. 5 TEM image of (a) Fe_2O_3 nanoparticles and (b) PB nanoparticles (c) GO–Fe_2O_3 nanocomposite (d) GO–PB nanocomposite.

3.2. Electrochemical characterisation

The electrochemical characterization of the modified electrodes in pH 7.0 PBS alone, and pH 7.0 PBS containing 5 mM Ferri/Ferro ($[Fe(CN)_6]^{3-/4-}$) redox probe was carried out using cyclic voltammetry (CV) and electrochemical impedance spectroscopy (EIS) techniques. The results obtained are presented in Fig. 6. The purpose of this study was to determine the electron transport properties of the modified electrodes/sensors. Fig. 6 showed the comparative current response of the modified electrodes in 5 mM $[Fe(CN)_6]^{3-/4-}$ redox probe and PBS electrolyte. Deposition of GO, Fe_2O_3 or PB on the Pt electrode enhanced the current of $[Fe(CN)_6]^{3-/4-}$ process as compared to the redox reaction on bare Pt electrode. Similar increase in current response was observed in the PBS electrolyte. In a related study, this behaviour has been attributed to the sheets like structure of rGO with high surface area[7] such as GO used in the present study, and good electrical conductivity of Fe_2O_3 and PB nanoparticles. Modification with the nanocomposite on the other hand significantly increase the current response (faster electron transport properties) of Pt–GO–Fe_2O_3 and Pt–GO–PB in both electrolytes, compared with the other electrodes investigated. The result obtained agreed with other studies reported in literature.[4,5,7,34] Other electrochemical features confirming successful modification of the bare Pt electrode with the synthesised nanomaterials are reported. For example in Fig. 6a, the redox peaks at I (0.2663 V) and II (0.1588 V) are attributed to the $[Fe(CN)_6]^{3-/4-}$ redox process. Similar redox process was observed for $[Fe(CN)_6]^{3-/4-}$ couple in the region 0.0–0.4 V (Fig. 6c) This couple is absent in 0.1 M PBS alone (Fig. 6b and d). Two additional redox peaks at II (0.4958 V) and III (0.8009 V) for the Pt–GO–Fe_2O_3 modified electrode (Fig. 6a), attributed to γ-Fe_2O_3/Fe_3O_4 and α-Fe_2O_3/FeOOH respectively confirmed successful modification of the Pt electrode with Fe_2O_3 nanoparticles. Same iron oxide oxidation peaks are seen at I (0.7887 V) and II (0.9621 V) for the same electrode in 0.1 M PBS (Fig. 6b) which further confirms successful transformation of the bare Pt electrode to Pt–GO–Fe_2O_3 modified electrode. Similarly, the redox peak at around 0.8 V, prominent on Pt–PB (inset in Fig. 6c), though not too obvious on Pt–GO–PB probably because of its large current, but absent on the bare Pt electrode confirm successful modification of Pt electrode with PB nanoparticles. The peak has been attributed to the formation of Prussian yellow (PY), an intermediate during PB oxidation.[61,62]

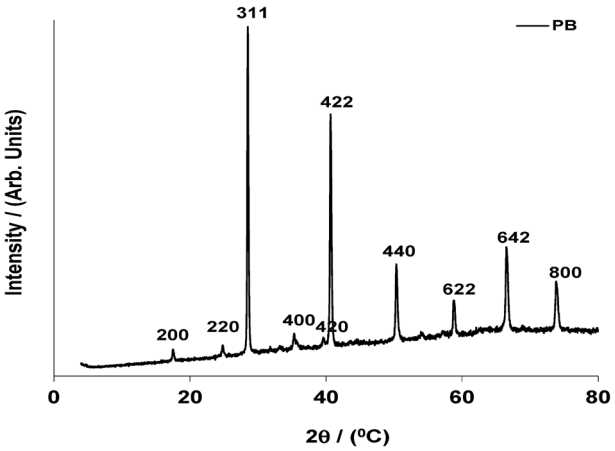

Fig. 4 XRD spectrum of Prussian blue (PB) nanoparticles.

3.3. Electrocatalytic oxidation of nitrite and nitric oxide

Fig. 7 and 8 present the oxidation potentials and the comparative current response of the electrodes in PBS containing 10^{-3} M nitrite (pH 7.0) and 10^{-3} M nitric oxide (pH 3.0). Nitrite exists as nitrite ion (NO_2^-) at physiological pH 7.0 where it gives its maximum peak current,[7] but disproportionate to produce the neutral nitric oxide (NO) at slightly acidic pH.[63]

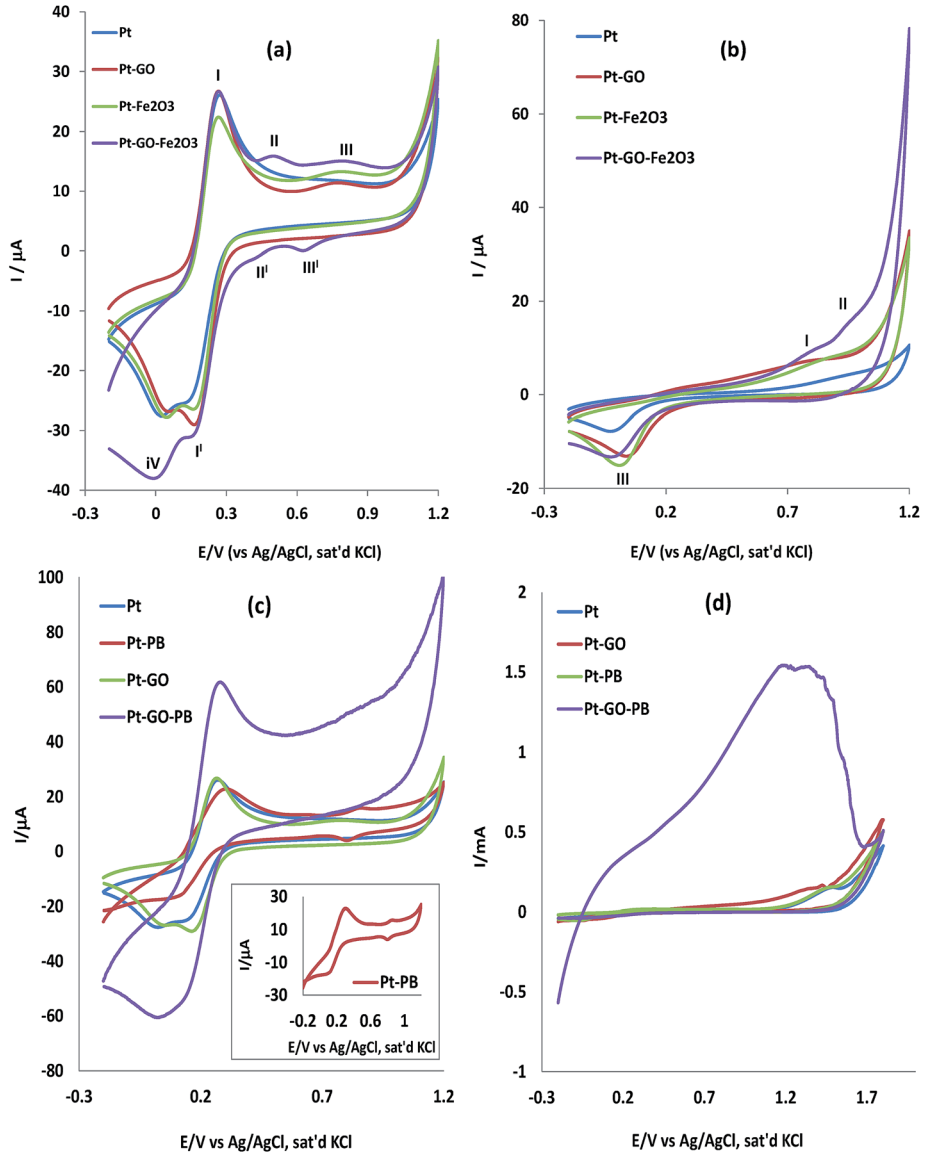

Fig. 6 Comparative cyclic voltammetric evolutions of Fe_2O_3 modified electrodes in (a) 5 mM $[Fe(CN)_6]^{4-}/[Fe(CN)_6]^{3-}$ (b) in pH 7.0 PBS (scan rate = 25 mV s^{-1}) (c) and (d) are comparative cyclic voltammetric evolutions of PB modified electrodes in 5 mM $[Fe(CN)_6]^{4-}/[Fe(CN)_6]^{3-}$ and in pH 7.0 PBS respectively (scan rate = 25 mV s^{-1}).

In Fig. 7a, an irreversible oxidation peak potential at *ca.* 0.8 V (*vs.* Ag|AgCl, sat'd KCl), equivalent to ~0.78 V (*vs.* SCE) was obtained for nitrite oxidation on the bare and the Fe_2O_3 modified electrodes. This potential is about 200 mV and 220 mV lower compared to 0.98 V (*vs.* SCE) and *ca.* 1.0 V (*vs.* SCE) reported for nitrite oxidation on carbon fibre microelectrode CFE[64] and on bare glassy carbon electrode (GCE)[65,66] respectively. The lower potential observed in this study may be due to the conductive and catalytic nature of the Pt electrode itself compared with the carbon based electrode, thereby fostering faster electronic interactions with the analyte at lower energy. After background current subtraction (Fig. 7b), nitrite oxidation current on the electrodes follows the order: Pt–GO–Fe_2O_3 (13.80 µA) > Pt–GO (7.80 µA) > Pt–Fe_2O_3 (7.30 µA) > Pt (6.30 µA). The Pt–GO–Fe_2O_3 electrode gave enhanced nitrite oxidation current which is twice that of the bare Pt electrode. Similar results have been obtained and reported in literature for modified electrodes.[29–38]

For example, Ning *et al.* reported the excellent electrocatalytic performance of Ag nanoparticles/dendrimer nanocomposite on GC electrode towards nitrite oxidation.[30] Similarly, Radhakrishnana *et al.* also reported excellent electrochemical performance of Fe_2O_3/rGO composite modified GC electrode towards nitrite, and its anti-interference ability against electroactive species and metal ions.[7] Cui *et al.* reported excellent catalytic ability of gold nanoparticles modified GCE (Au/GCE) toward the oxidation of nitrite compared with bare GCE.[67] Improved electrochemical detection of nitrite and nitrate in water using Pt electrode modified with cellulose acetate membrane or with poly (1,8-diaminonaphthalene) film has also been reported.[68]

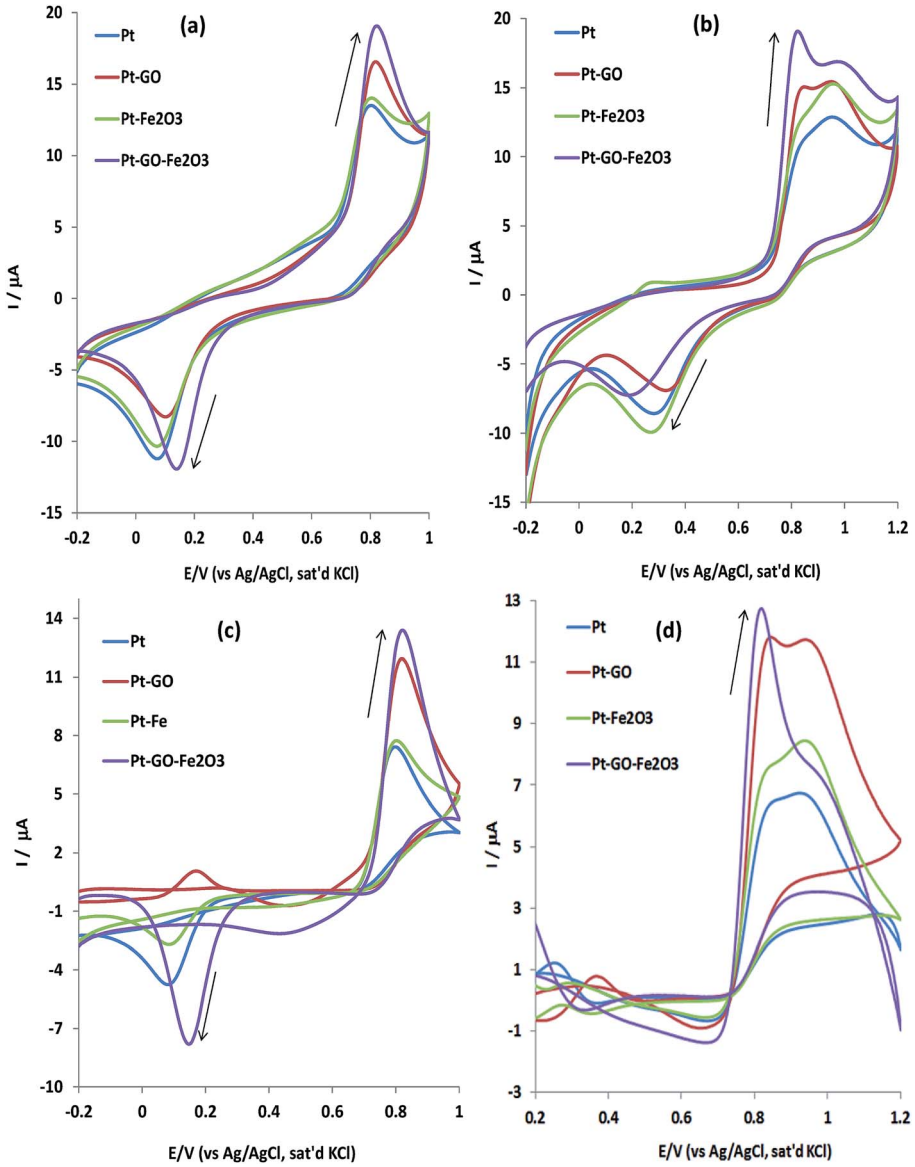

Fig. 7 Comparative current response of Fe_2O_3 modified electrodes in (a) 10^{-3} M NO_2^- in pH 7.0 PBS (b) 10^{-3} M NO in pH 3.0 PBS (scan rate = 25 mV s^{-1}) (c) and (d) are comparative current response of Fe_2O_3 modified electrodes in 10^{-3} M NO_2^- and 10^{-3} M NO respectively (after background current subtraction).

The Pt–GO–Fe_2O_3 nanocomposite electrode also demonstrated enhanced NO current response at lower oxidation potential (0.82 V) compared to bare Pt electrode (0.86 V), Pt–Fe (0.92 V) and Pt–GO (0.95 V) (Fig. 7c). After background current subtraction (Fig. 7d), NO oxidation current on the electrodes follow the order: Pt–GO–Fe_2O_3 (11.60 μA) > Pt–GO (8.77 μA) > Pt–Fe_2O_3 (6.43 μA) > Pt (6.12 μA). The enhanced NO current response at Pt–GO–Fe_2O_3 electrode, which is twice that at bare Pt is attributed to the synergy between GO–Fe_2O_3 leading to the improved electrocatalytic properties of the surface nanocomposite material.[7] The lower NO oxidation potential on this electrode suggest large surface area created by the porous GO material allowing easy contact of the analyte with the Fe_2O_3 catalyst thus faster reaction kinetics.

Similarly using PB modified electrodes, Pt–GO–PB nanocomposite modified electrode gave the highest NO_2^- and NO oxidation currents (Fig. 8a and b). After background current subtraction (Fig. 8c and d), NO_2^- and NO oxidation current at Pt–GO–PB electrode are 11.40 μA and 12.59 μA respectively which is approximately twice (2×) their oxidation current at the bare Pt electrode signifying the importance of chemically modified electrodes in electrocatalysis. Similar factors such as presence of porous GO sheet, increase electrode surface area and the electrical conductive nature of the PB nanoparticles could be responsible for the improved response of the analyte at the electrode. The result obtained in this study agreed with similar observation for nitrite oxidation on gold nanoparticles choline chloride glassy carbon modified electrode (nano-Au/Ch/GCE), which was reported to be better compared to the bare gold, or nano-Au/GCE or Ch/

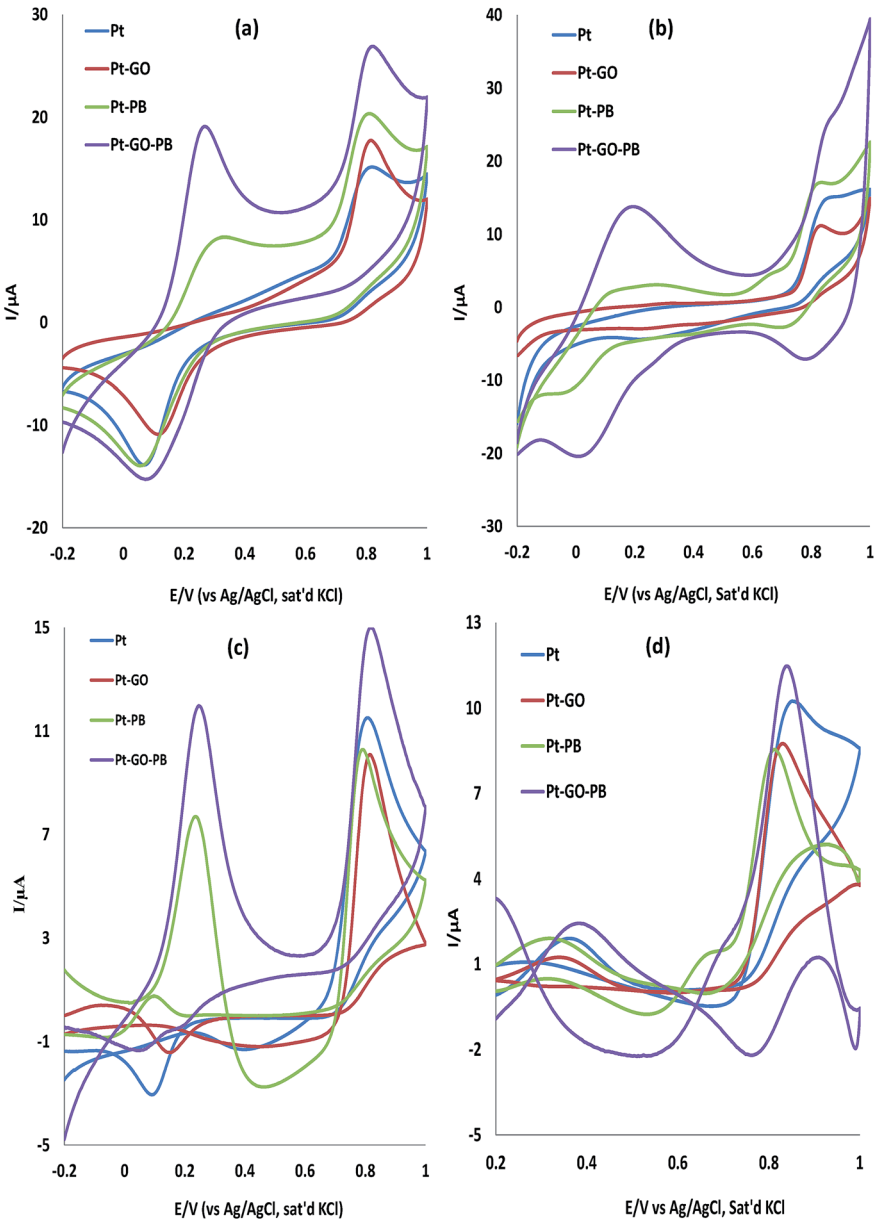

Fig. 8 Comparative current response of PB modified electrodes in (a) 10^{-3} M NO_2^- in pH 7.0 PBS (b) 10^{-3} M NO in pH 3.0 PBS (scan rate = 25 mV s^{-1}) (c) and (d) are comparative current response of PB modified electrodes in 10^{-3} M NO_2^- and 10^{-3} M NO respectively (after background current subtraction).

GCE alone[66] signifying the importance of chemically modified electrodes in catalysis. Since Pt–GO–Fe_2O_3 and Pt–GO–PB have demonstrated excellent catalytic properties towards NO_2^- and NO oxidation in this study, further studies were not carried out using these electrodes unless otherwise stated.

3.4. Electrochemical impedance spectroscopy (EIS) studies

The electrocatalytic oxidation of NO_2^- and NO at Pt–GO–Fe_2O_3 and Pt–GO–PB modified electrodes was investigated using the electrochemical impedance spectroscopy (EIS) technique. The Nyquist and Bode plots obtained for Pt–GO–Fe_2O_3 electrode in NO_2^- and NO respectively (at fixed potential of 0.8 V *vs.* Ag/AgCl, sat'd KCl) and between 10 KHz and 1 Hz are presented in Fig. 9. Similar plots (not shown) were obtained using Pt–PB and Pt–GO–PB electrode in the analytes. All the obtained spectra were first subjected to the Kramers–Kronig (K–K) test. The main essence of the K–K test is simply to check whether the measured impedance spectra comply with the assumptions of the well-known K–K transformation, *viz.* (i) that the impedimetric response is only related to the excitation signal; (ii) that the impedimetric response is linear or the perturbation is small, *e.g.*, <10 mV, for non-linear systems; (iii) that the system does not change with time, say due to ageing, temperature changes, non-equilibrium conditions, *etc.*; and (iv) that the system is finite for all values of ω, including zero and infinity.[69,70] Failure of the K–K test, signified by a large value of pseudo χ^2 is usually an indication that no good fit can be obtained using the

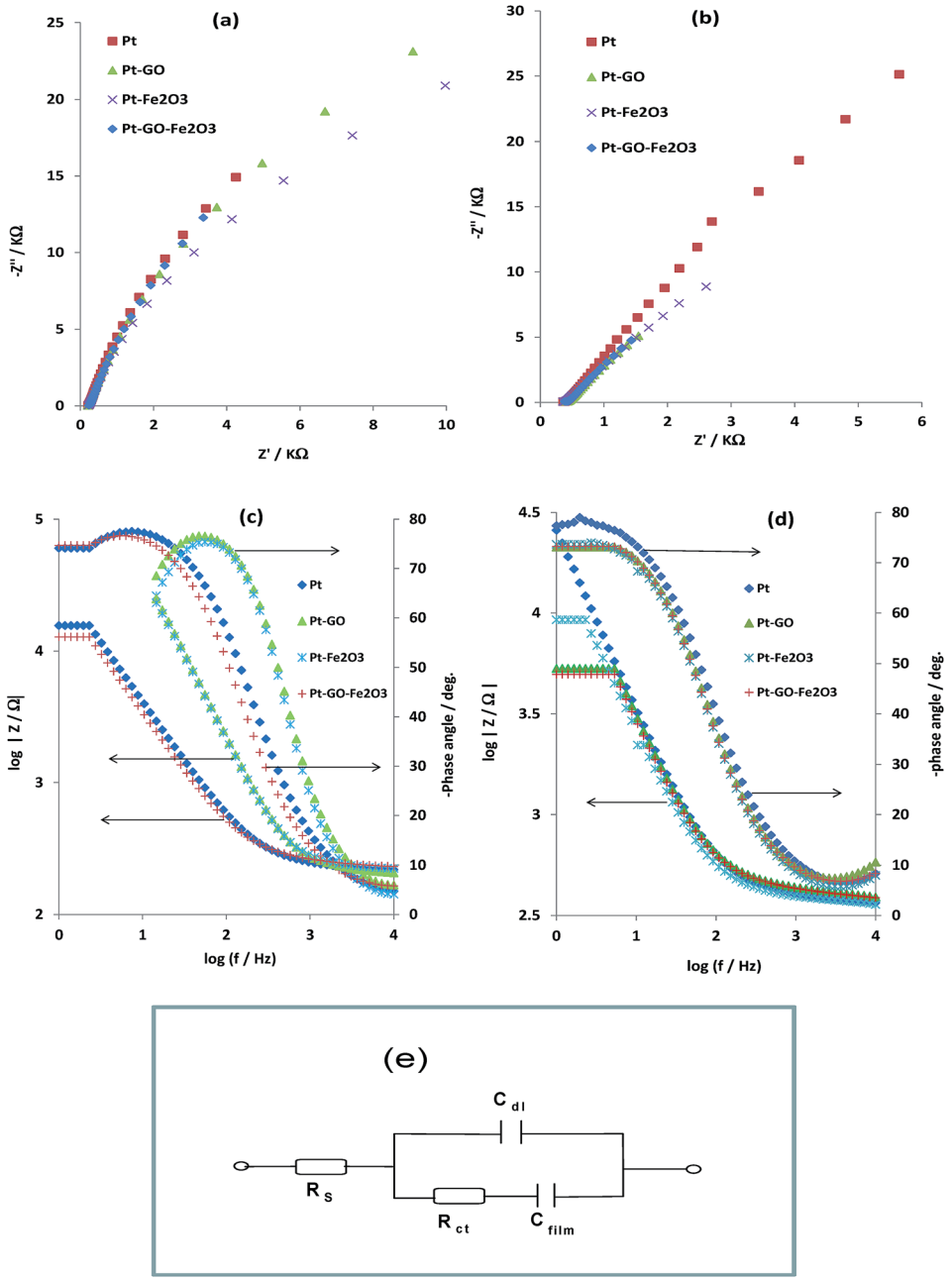

Fig. 9 Typical Nyquist plots obtained for Pt–GO–Fe_2O_3 electrode in (a) 1.0 mM NO_2^- and (b) 1.0 mM NO solutions at a fixed potential of 0.8 V (*vs.* Ag|AgCl, sat'd KCl) (c) and (d) are the Bode plots obtained for Pt–GO–Fe_2O_3 electrode in NO_2^- and NO respectively showing the plots of phase angle/deg. *vs.* log(*f*/Hz), and the plot of log|*Z*/Ω| *vs.* log(*f*/Hz) (e) represents the circuit used in the fitting of the EIS data in (a) and (b).

electrical equivalent circuit's methods. It should be noted that aside from visual inspection of goodness of the fitting lines, two accurate ways to establish how well the modelling functions reproduce the experimental data sets are the relative error estimates (in %) and chi-square functions (χ^2),[71] which is the sum of squares of the relative residuals (*i.e.*, sum of the real and imaginary χ^2), easily obtained from the K–K test.

The impedance data was satisfactorily fitted with a circuit model (Fig. 9e) and the data obtained is presented in Table 1. In this circuit model, R_s is the solution resistance, C_{dl} represents the double layer capacitance, C_{film} describes the high pseudocapacitive nature of the system and R_{ct} is the charge transfer resistance of the electrode.[29]

From the EIS result (Table 1), the R_{ct} values for the Pt–GO–Fe_2O_3 electrode in NO_2^- (1.57 Ω cm^2) and NO (0.45 Ω cm^2); and Pt–GO–PB electrode in NO_2^- (0.94 Ω cm^2) and NO (0.15 Ω cm^2) are lower compared with 1.97 Ω cm^2 (NO_2^-) and 0.55 Ω cm^2 (NO) recorded for the analytes on the bare Pt electrode. Similar lower R_{ct} value was reported for Fe_2O_3/rGO/GCE modified electrode towards nitrite oxidation due to the modifier ability to form good electron pathways between the electrode and electrolyte thus making the modified electrode a good platform for sensing

Table 1 Impedance data obtained for the electrodes in 10^{-3} M nitrite (pH 7.0 PBS) and 10^{-3} M nitric oxide (pH 3.0 PBS) respectively (at 0.8 V *vs.* Ag|AgCl sat'd KCl). Note that the values in parentheses are percentage errors of the data fitting

	Impedance parameters			
Electrodes	R_s (Ω cm^2)	C_{dl} (μF)	R_{ct} (Ω cm^2)	C_{film} (μF)
NO_2^-				
Pt	23.72 (0.290)	3.490 (3.234)	1.97 (1.183)	4.62 (11.805)
Pt–GO	23.0 (0.296)	4.350 (3.482)	2.20 (1.999)	3.031 (17.881)
Pt–Fe_2O_3	24.27 (0.261)	4.67 (3.010)	2.65 (1.444)	4.59 (19.656)
Pt–GO–Fe_2O_3	25.51 (0.294)	4.23 (3.567)	1.57 (1.270)	5.49 (12.114)
Pt–PB	25.96 (0.323)	6.34 (4.442)	0.86 (1.148)	12.22 (12.976)
Pt–GO–PB	22.73 (0.307)	6.09 (3.999)	0.94 (1.087)	11.41 (12.467)
NO				
Pt	39.60 (0.199)	3.67 (3.829)	0.55 (1.881)	2.20 (8.723)
Pt–GO	42.60 (0.490)	4.97 (8.932)	0.49 (1.475)	15.11 (12.713)
Pt–Fe_2O_3	39.50 (0.273)	5.67 (4.204)	1.05 (1.298)	7.62 (11.573)
Pt–GO–Fe_2O_3	42.00 (0.492)	5.30 (9.198)	0.45 (1.493)	16.15 (12.717)
Pt–PB	43.20 (0.312)	5.64 (5.867)	0.44 (1.175)	11.76 (11.151)
Pt–GO–PB	40.90 (0.283)	13.77 (8.354)	0.15 (1.179)	37.3 (11.054)

applications.[7] Similar reason was attributed to the lower R_{ct} observed for the nanocomposite electrodes. The results obtained in this study clearly indicate improve electrical conductivity, enhanced electron transport and excellent electrocatalytic oxidation of these important analyte at Pt–GO–Fe_2O_3 and Pt–GO–PB electrodes, which further confirm the CV results trend reported above.

From the Bode plots of phase angle *vs.* log(*f*/Hz) (Fig. 9c and d) a phase angle of ~−75 and −70 (at 1.0 Hz) was obtained for Pt–GO–Fe_2O_3 electrode in NO_2^- and NO respectively. Similarly, at the same frequency, a phase angle of ~−72° and −36° (not shown) was obtained for Pt–GO–PB electrode in the analytes. These phase angles are lower compared with that of the bare Pt (Fig. 9c and d).

This result implies that the Pt–GO–Fe_2O_3 and Pt–GO–PB electrodes is less capacitive compared with the bare and their pseudocapacitive behaviour can be attributed to the conductive nature of the Fe_2O_3 and PB nanoparticles. A phase angle of −90° is expected for a pure capacitive behaviour.

From the plots of log|*Z*/Ω| *vs.* log(*f*/Hz) (Fig. 9c and d), Pt–GO–Fe_2O_3 electrode gave slope values (*n*) of 0.7724 (R^2 = 0.9924) and 0.7019 (R^2 = 0.9901) in NO_2^- and NO respectively, while Pt–GO–PB electrode gave slope values of 0.8763 (R^2 = 1) and 0.5813 (R^2 = 0.9972) in NO_2^- and NO. Slope (*n*) has values $-1 \leq n \leq 1$. A slope value of 1.0 is expected for a pure capacitive behaviour.[29] Therefore results obtained in this study further confirm the pseudocapacitive nature of the electrode towards the analytes oxidation.

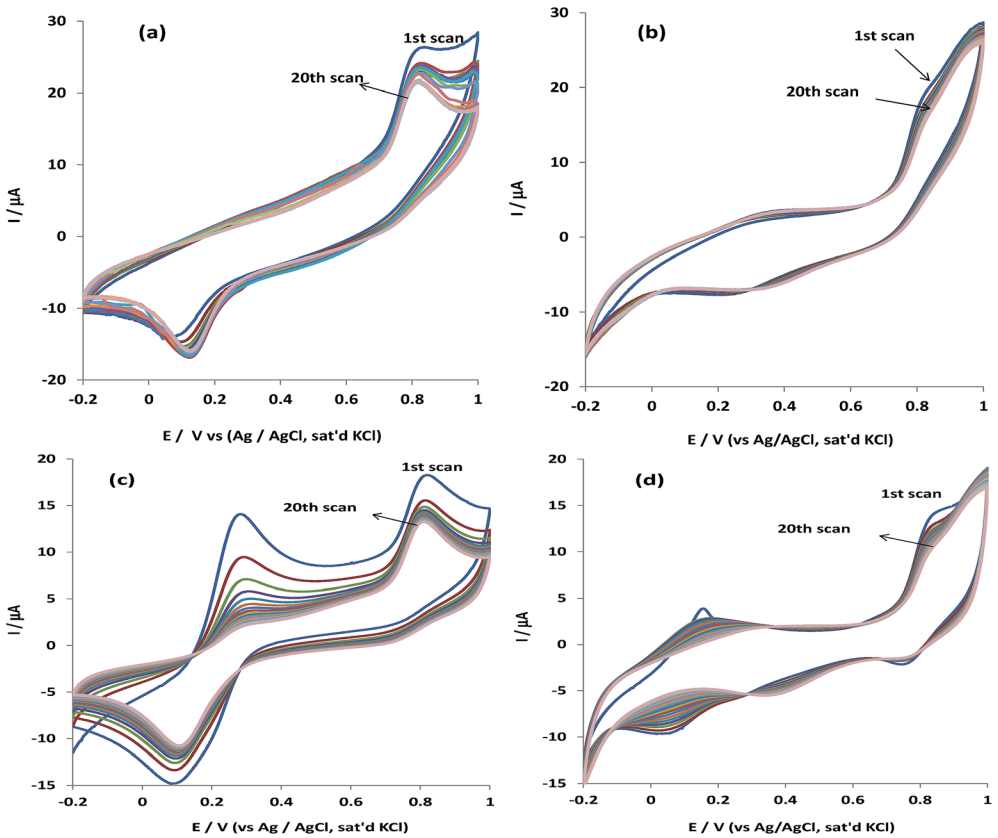

Fig. 10 Current response (20 scans) of Pt–GO–Fe_2O_3 electrode in (a) 0.1 M pH 7.0 PBS containing 10^{-3} M NO_2^-. (b) pH 3.0 PBS containing 10^{-3} M NO (scan rate: 25 mV s^{-1}). Current response (20 scans) of Pt–GO–PB electrode in (c) 0.1 M pH 7.0 PBS containing 10^{-3} M NO_2^-. (d) pH 3.0 PBS containing 10^{-3} M NO (scan rate: 25 mV s^{-1}).

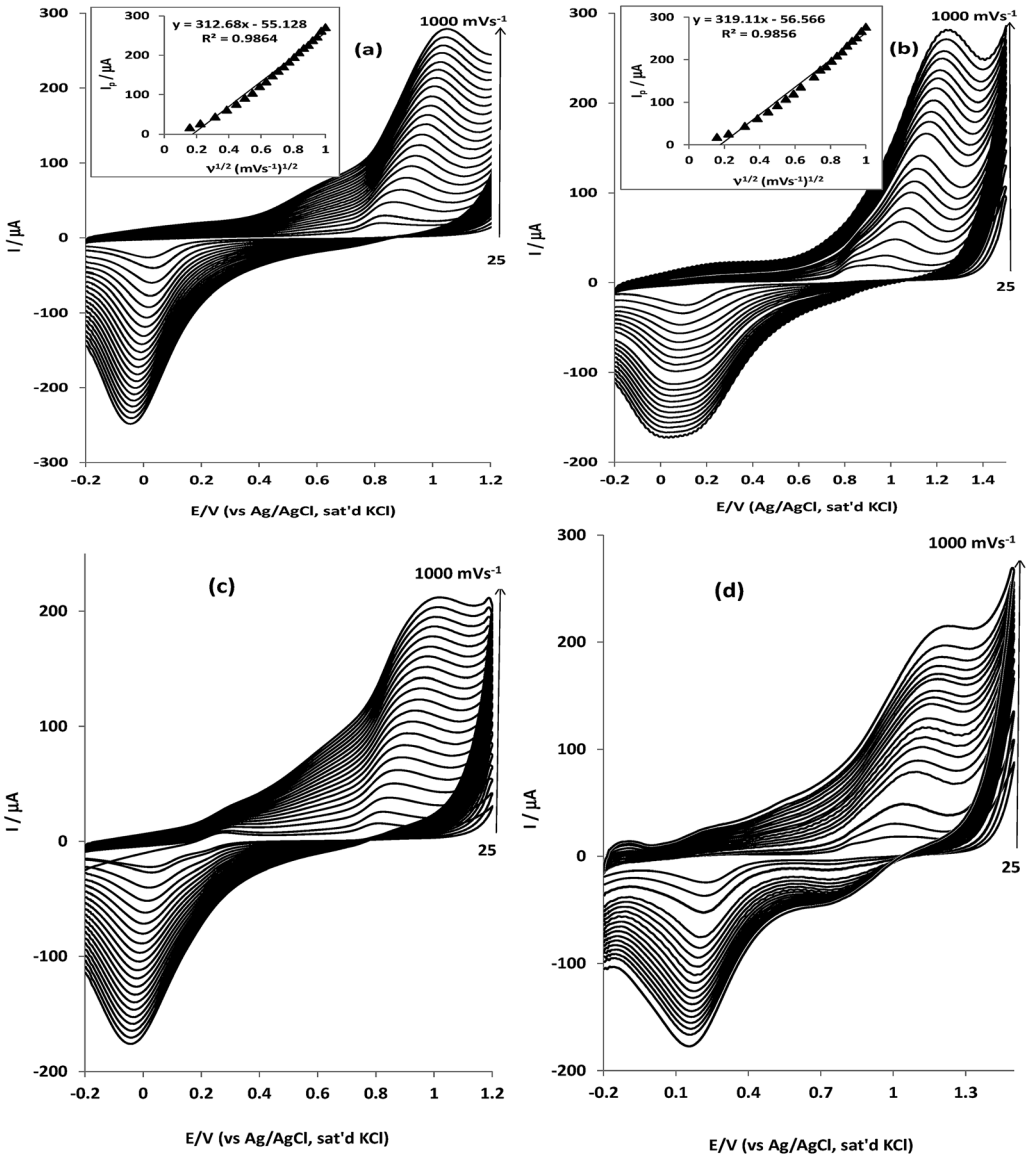

Fig. 11 Cyclic voltammetric evolutions of Pt–GO–Fe_2O_3 electrode obtained in 0.1 M PBS containing (a) 10^{-3} M NO_2^- (pH 7.0), (b) 10^{-3} M NO (pH 3.0) (scan rate range 25–1000 mV s^{-1}; inner to outer). Cyclic voltammetric evolutions of Pt–GO–PB electrode obtained in 0.1 M PBS containing (c) 10^{-3} M NO_2^- (pH 7.0), (d) 10^{-3} M NO (pH 3.0) (scan rate range 25–1000 mV s^{-1}; inner to outer).

3.5. Stability study

The resistance of Pt–GO–Fe_2O_3 and Pt–GO–PB electrodes towards NO_2^- and NO oxidation product fouling effect was investigated by running (20 scans) the electrodes in 10^{-3} M NO_2^- and 10^{-3} M NO respectively using cyclic voltammetry technique (Fig. 10a and b). After 20 scans, Pt–GO–Fe_2O_3 electrode showed relatively low drop in NO_2^- and NO oxidation current, 17.2 and 15.9% respectively indicating the stability of the electrode towards fouling effect. The result also suggests some levels of adsorption of the analyte, or their oxidation intermediates at the electrode surface. Similar results were obtained for Pt–GO–PB electrode in NO_2^- and NO (Fig. 10c and d) but with higher current drop, 27.5 and 25.2% for NO_2^- and NO respectively. From this study, Pt–GO–Fe_2O_3 electrode demonstrated better performance towards the analyte compare with Pt–GO–PB electrode. Generally, the adsorptive nature of the electrodes towards the analyte can be attributed to the porous GO assembly as adsorptive behaviour of related porous CNT modified electrode has been linked with the CNT layer.[72]

However, the higher current drop noticed at Pt–GO–PB electrode can be attributed to the mixed-valence charge-transfer behaviour of the [Fe(II)–C–NFe(III)] complex, or the strong interaction between the lone pair of electron on the Prussian blue N atom and the analyte or its intermediates, and the π–π interaction of the C≡N groups of the PB and the analyte or its intermediates. This could lead to adsorption of the species on the catalyst, thus the drop experienced.

After electrochemical cleaning of the used electrode in pH 7.0 PBS (repetitive cycling, 30 scans), a current recovery of *ca.*

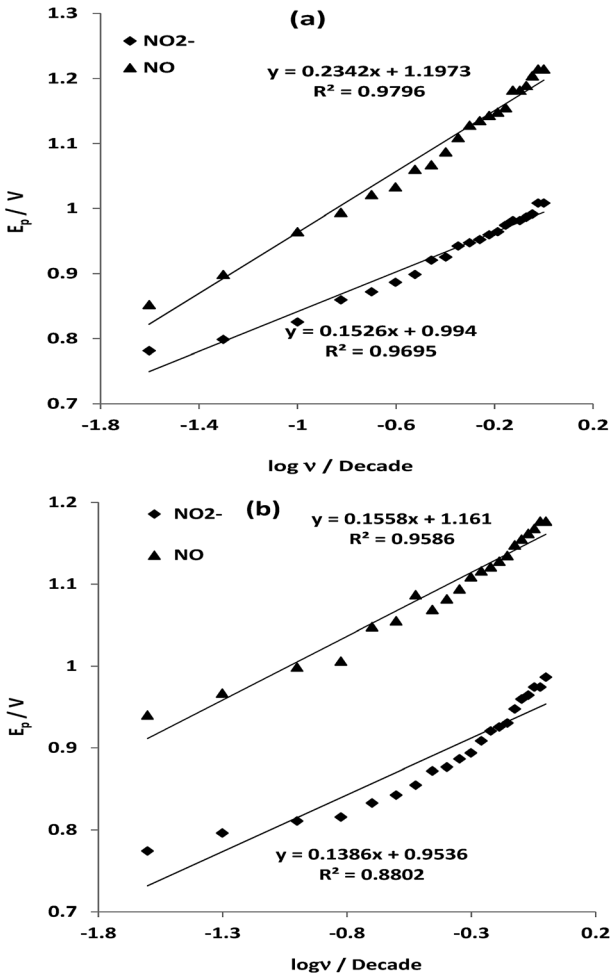

Fig. 12 (a) Plots of peak potential (E_p) *versus* log ν for 10^{-3} M NO_2^- and NO respectively obtained using Pt–GO–Fe_2O_3 electrode. (b) Plots of peak potential (E_p) *versus* log ν for 10^{-3} M NO_2^- and NO respectively obtained using Pt–GO–PB electrode.

85–90% was obtained suggesting that the initial current drop was due to simple physical adsorption (physisorption) of the analyte or their intermediate oxidation products on the electrode. The result therefore suggests that the electrode is electrochemically stable and can be reused after an experiment. It can also be used as disposable electrodes such as screen-printed electrode. The electrode also demonstrated an insignificant drop in current response due to NO_2^- and NO oxidation after storage in phosphate buffer solution (pH 7.0) in a refrigerator (at 4 °C) for up to four weeks.

3.6. Effect of scan rate

Scan rate study (scan rate, 25–1000 mV s^{-1}) in the analyte was carried out using cyclic voltammetry technique (Fig. 11). Pt–GO–Fe_2O_3 electrode gave NO_2^- (Fig. 11a) and NO (Fig. 11b) oxidation current which increases with increasing scan rate suggesting diffusion controlled process. Similarly, the anodic peak current (I_{pa}) was directly proportional to the square root of scan rate ($\nu^{1/2}$) (inset in Fig. 11a and b) but with negative intercept. Randles–Sevčik equation for an anodic oxidation process with a zero intercept suggests a true and complete diffusion control process.[73] Therefore, the negative intercept from the plot of I_{pa} *versus* $\nu^{1/2}$ suggests that the electrode reaction is not a pure diffusion-controlled process but characterized with some level of adsorption of NO_2^- and NO or their intermediate oxidation product at the electrode. Similar results were obtained for scan rate study of Pt–GO–PB electrode in the analyte (Fig. 11c and d). The result further support the adsorption phenomenon already indicated under stability study above. In a related study, oxidation of nitrite has been described at the Fe_2O_3/rGO modified GC electrode as diffusion controlled process.[7] The difference could be due to electrode method of preparation, porosity, conformation and the catalyst–analyte interaction. For example, electrode porosity has been associated with adsorption and high Tafel values as obtained in this study and discussed below.

Using the Tafel equation for an irreversible-diffusion controlled process,[73]

$$E_p = K + \frac{2.303RT}{2(1-\alpha)n_\alpha F}\log \nu \quad (1)$$

or

$$E_p = K + \frac{b}{2}\log \nu \quad (2)$$

where α is the transfer coefficient, b is the Tafel value, n_α is the number of electrons involved in the rate-determining step. R, T and F are gas constant, temperature and Faraday constant, respectively.

A linear plot for E_{pa} *vs.* the log ν was obtained for Pt–GO–Fe_2O_3 (Fig. 12a) and Pt–GO–PB (Fig. 12b) modified electrodes in NO_2^- and NO respectively. From the slope of the Tafel plots (E_p *vs.* log ν), the Tafel values b of 468.4 and 305.2 mV dec^{-1} were obtained in NO_2^- and NO using Pt–GO–Fe_2O_3 electrode, while Tafel values of 311.5 and 277.2 mV dec^{-1} were obtained in NO_2^- and NO respectively at the Pt–GO–PB modified electrode. These values are higher than the theoretical value of 118 mV dec^{-1} for a one-electron process involved in the rate-determining step. Therefore, such high Tafel values are attributed to the adsorption of reactants or intermediates on the electrode surfaces and/or reactions occurring within a porous electrode structure.[74] It is interesting to mention that despite the high Tafel values recorded at the Pt–GO–Fe_2O_3 electrode, the electrode still gave better performance towards NO_2^- and NO oxidation in terms of oxidation potential, current recovery, stability and resistance to fouling effects as compared with Pt–GO–PB modified electrode which may be attributed to the high electrical conductivity and ionic properties of the Fe_2O_3 catalyst. The higher Tafel values at the electrode could be due to oxidation of more NO_2^- and NO molecules. The higher Tafel values for NO_2^- as compared to NO can also be attributed to the extra oxygen atom and charge on NO_2^- molecule.

3.7. Concentration study

The effect of current response on varying concentrations of NO_2^- and NO using linear sweep voltammetry (LSV) technique (Fig. 13) was carried out. The linear sweep voltammograms were

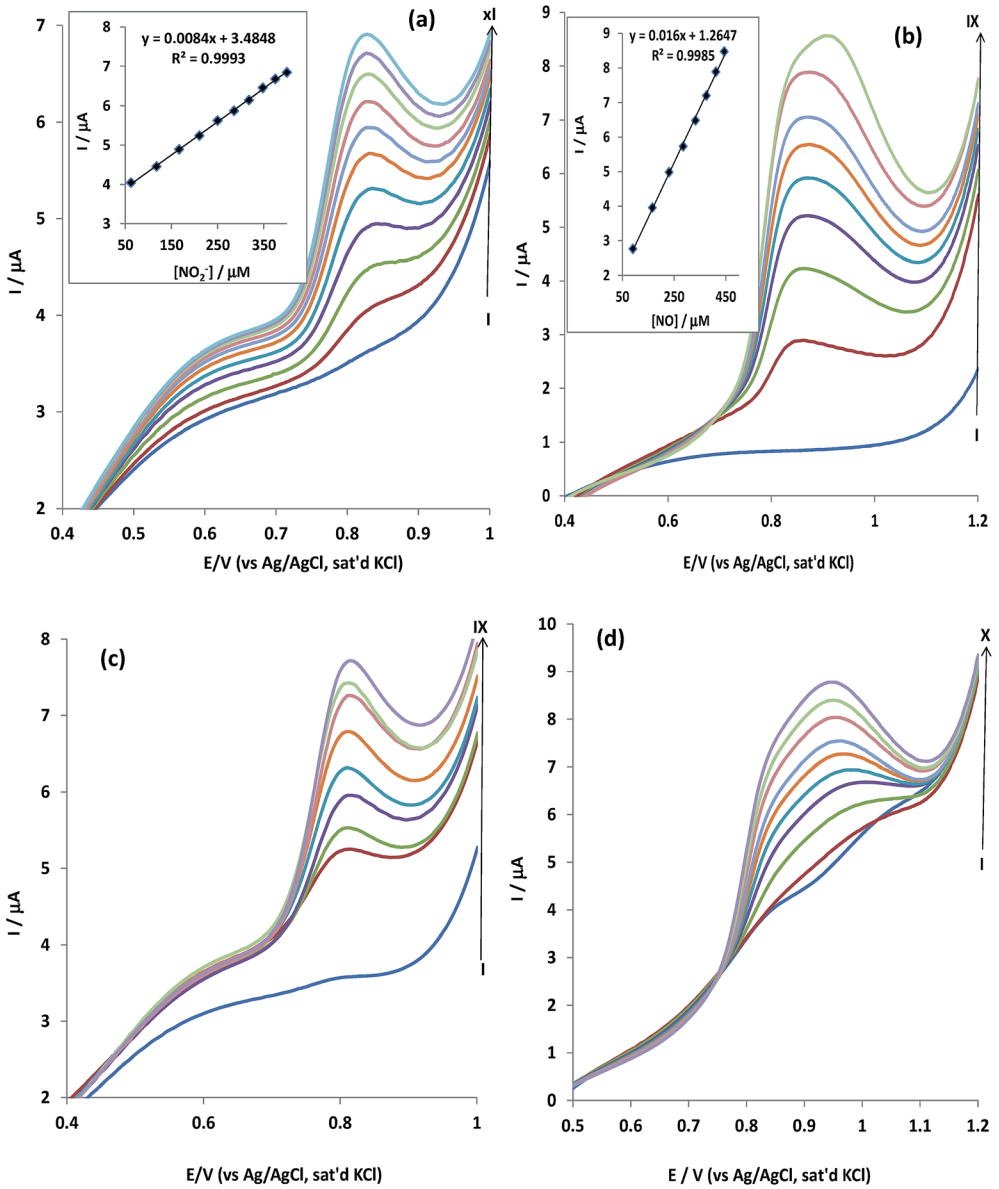

Fig. 13 Typical linear sweep voltammograms of Pt–GO–Fe_2O_3 electrode in (a) pH 7.0 PBS containing different concentrations of NO_2^- (0.0, 62.5, 117.7, 166.7, 210.5, 250.0, 286.0, 318.2, 347.8, 375.0 and 400.0 μM) (i to xi) and (b) pH 3.0 PBS containing different concentrations of NO (0.0, 90.9, 166.7, 230.8, 285.7, 333.3, 375.0, 411.8 and 444.4 μM) (i to ix). Insets in (a) and (b) are the plots of current response *vs.* nitrite concentration. Typical linear sweep voltammograms of Pt–GO–PB electrode in (c) pH 7.0 PBS containing different concentrations of NO_2^- (0.0, 117.7, 166.7, 210.5, 250.0, 318.2, 347.8, 375.0 and 400.0) μM (i to ix) and (d) pH 3.0 PBS containing different concentrations of NO (0.0, 90.9, 166.7, 230.8, 285.7, 333.3, 375.0, 444.4, 473.7 and 500.0 μM) (i to x).

obtained after stirring the mixture thoroughly. Fig. 13a and b are the voltammograms obtained in NO_2^- and NO using Pt–GO–Fe_2O_3 modified electrode, while Fig. 13c and d represent their corresponding voltammograms using Pt–GO–Fe_2O_3 modified electrode. The inset in Fig. 13a and b represent the calibration curve for the plot of peak current (I_p) *versus* NO_2^- and NO concentration respectively. Similar plots (not shown) were obtained for Fig. 13c and d. The measured peak currents were found to be linear with increasing concentrations. The detection limit was calculated based on the relationship LoD = $3.3\delta/m$ where δ is the relative standard deviation of the intercept of the *y*-coordinates from the line of best fit, and *m* the slope of the same line.[75] The limit of detection and sensitivity of the Pt–GO–Fe_2O_3 electrode in NO_2^- and NO are 6.60 μM (0.0084 μA μM^{-1}) and 13.04 μM (0.0160 μA μM^{-1}) respectively. Similarly, the limit of detection and sensitivity of the Pt–GO–PB electrode in NO_2^- and NO are 16.58 μM (0.0093 μA μM^{-1}) and 16.50 μM (0.0091 μA μM^{-1}) respectively. The 6.60 μM reported for NO_2^- agreed closely with 5.61 μM recently reported[29] with a factor of 100 lower compared with 4.5×10^{-4} M and 1×10^{-5} M reported on poly(4-aminoacetanilide) film modified carbon paste electrode (PPAA/CPE) using cyclic voltammetry (CV) and hydrodynamic amperometry methods respectively.[38] Also, the 13.04 μM for NO agreed closely with 8.03 μM recently reported.[29]

From the chronoamperometric study (not shown) and using eqn (3):[75]

$$\frac{I_{cat}}{I_L} = \pi^{1/2}(kC_o t)^{1/2} \quad (3)$$

where I_{cat} and I_L are the currents in the presence and absence of the analyte, k is the catalytic rate constant, C_o is the bulk concentration and t is the elapsed time. From the plot of I_{cat}/I_L *vs.* $t^{1/2}$, the catalytic rate constant k obtained for Pt–GO–Fe_2O_3 in 10^{-3} M NO_2^- and 10^{-3} M NO are 5.39 and 8.73×10^5 cm^3 mol^{-1} s^{-1}, while the k values for Pt–GO–PB electrode in NO_2^- and NO are 6.42 and 12.57×10^4 cm^3 mol^{-1} s^{-1} respectively. The higher values of k_{cat} for Pt–GO–Fe_2O_3 electrode in the analytes further corroborates its excellent electrocatalysis, stability, current recovery and lower limit of detection obtained in this study as compared with Pt–GO–PB electrode. The k_{cat} values obtained for Pt–GO–Fe_2O_3 is in the 10 order of magnitude higher than 0.32 and 0.34×10^5 cm^3 mol^{-1} s^{-1} reported for the analytes on EPPGE-SWCNT-Co electrode modified by electrodeposition,[29] and 8.4×10^4 cm^3 mol^{-1} s^{-1} at PPAA/CPE made by electropolymerisation. On the other hand, Pt–GO–PB electrode k_{cat} values agreed closely with the reported values at EPPGE-SWCNT-Co electrode.[29] The difference in the magnitude of k_{cat} could be due to the different electrode modifiers, the different experimental conditions and their degree of interaction with the analytes. However, higher k_{cat} values reported in this work could be due to the ability of GO to form a strong and efficient synergy with PB and Fe_2O_3 in their respective nanocomposite thus enhancing their catalysis towards NO_2^- and NO.

Due to the adsorptive nature of NO_2^- and NO on the electrode as indicated by the Tafel values, linear sweep or stripping voltammetry (LSV) technique was employed to monitor the extent of adsorption of these analytes at different concentrations using data from the concentration studies above. From Langmuir adsorption isotherm theory (eqn (4),[76]), where I_{cat}, I_{max} and β means catalytic current, maximum current and adsorption equilibrium constant, the plot of the ratio of [nitrite]/I_{cat} against [nitrite] gave a straight line (not shown) which confirms an adsorption controlled electrode process.

$$\frac{[\text{nitrite}]}{I_{cat}} = \frac{1}{\beta I_{max}} + \frac{[\text{nitrite}]}{I_{max}} \quad (4)$$

From the slope and the intercept of the curve obtained, the adsorption equilibrium constant β for NO_2^- and NO at the Pt–GO–Fe_2O_3 electrode is 10.29×10^3 M^{-1} and 3.26×10^3 M^{-1}. Similarly, β of 7.47×10^3 M^{-1} (NO_2^-) and 6.48×10^3 M^{-1} (NO) was obtained for the analyte at Pt–GO–PB electrode. The higher β of NO_2^- at Pt–GO–Fe_2O_3 electrode further support its high Tafel values obtained above.

From the relationship:

$$\Delta G^0 = -RT \ln \beta \quad (5)$$

where R and T have their usual meanings, the Gibbs free energy change due to adsorption (ΔG^0) was estimated from β values as −22.89 (NO_2^-) and −20.04 kJ mol^{-1} (NO) at Pt–GO–Fe_2O_3 electrode, and −22.10 (NO_2^-) and −21.74 kJ mol^{-1} (NO) at Pt–GO–PB electrode. The ΔG^0 are not significantly different probably because of similar reaction mechanism of the two analytes on the electrodes to give common stable oxidation product (NO_3^-). However, the ΔG^0 are quite higher (2×) compared to the previously reported values using EPPGE-SWCNt-Co modified electrode for electrocatalytic oxidation of NO_2^- and NO.[29]

3.8. The interference studies

The interference effect ions such as Cl^-, NO_3^-, SO_3^{2-} and SO_4^{2-} on the determination of nitrite (NO_2^-) and nitric oxide (NO) at Pt–GO–Fe_2O_3 and Pt–GO–PB electrodes was investigated. The experiment was conducted by adding various ions into PBS solution containing 1 mM nitrite (pH 7.0) and 1 mM nitric oxide (pH 3.0) respectively and the results obtained are summarized in Table 2. It was observed that most ions did not show any

Table 2 Effect of foreign ions on the amperometric detection of 1 mM nitrite (NO_2^-) and 1 mM nitric oxide (NO)

Effect of foreign ions on the amperometric detection of NO_2^- and NO on Pt–GO–Fe_2O_3 electrode

Ions added	Relative current response[a] (%) at different molar ratios of ([NO_2^-]) : ([added ions])	
	1 : 1	1 : 10
Cl^-	100 ± 7.15	100 ± 7.15
NO_3^-	85.7 ± 7.14	85.71 ± 7.14
SO_3^{2-}	100 ± 7.15	114.28 ± 0.01
SO_4^{2-}	100 ± 7.15	85.71 ± 7.14
	Relative current response[a] (%) at different molar ratios of ([NO]) : ([added ions])	
	1 : 1	**1 : 10**
Cl^-	100 ± 7.15	71.43 ± 0.01
NO_3^-	142.86 ± 7.15	71.43 ± 7.15
SO_3^{2-}	85.78 ± 0.04	457.1 ±
SO_4^{2-}	85.78 ± 0.04	85.7 ± 7.15

Effect of foreign ions on the amperometric detection of NO_2^- and NO on Pt–GO–PB electrode

Ions added	Relative current response[a] (%) at different molar ratios of ([NO_2^-]) : ([added ions])	
	1 : 1	1 : 10
Cl^-	85.7 ± 7.14	85.7 ± 0.04
NO_3^-	77.1 ± 1.4	70 ± 5.72
SO_3^{2-}	71.4 ± 0.01	485.7 ± 7.5
SO_4^{2-}	114.3 ± 0.05	77.14 ± 2.86
	Relative current response[a] (%) at different molar ratios of ([NO]) : ([added ions])	
	1 : 1	**1 : 10**
Cl^-	114.2 ± 7.15	100 ± 7.15
NO_3^-	114.28 ± 0.01	85.7 ± 7.15
SO_3^{2-}	128.6 ± 0.01	114.28 ± 7.28
SO_4^{2-}	85.71 ± 7.15	100 ± 7.15

[a] Relative response (%) = $I_{nitrite(or\ nitric\ oxide)}$ + added ions/$I_{nitrite(or\ nitric\ oxide)}$ obtained from at least three repetitive experiments.

interference effect at 1 : 1 ratio of NO_2^- and NO to that of the interfering ion, except at Pt–GO–PB electrode where approximately 70% recovery for NO_2^- current was recorded in the presence of NO_3^-, SO_3^{2-} ions. However, at 10-fold concentration of interference ions, SO_3^{2-} ion shows serious interference. Indeed, this result is unique and presents a good NO_2^- and NO current signals even in the presence of 10-fold concentration of the interference ions.

Based on reports on NO_2^-,[7] and NO_3^- oxidation on modified electrodes,[77] the mechanism below was proposed for NO_2^- oxidation at Pt–GO–PB electrode:

$$[GO\text{–}Fe^{3+}/Fe^{2+}]_{film} + H_2O \rightarrow [GO\text{–}Fe^{3+}/Fe^{3+}]_{film(aq)} + e^- \quad (6)$$

$$[GO\text{–}Fe^{3+}/Fe^{3+}]_{film(aq)} + NO_2^- \rightleftarrows [GO\text{–}Fe^{3+}/Fe^{3+}]_{film} + NO_2 + e^- \text{ (slow)} \quad (7)$$

$$2NO_2 + H_2O \rightleftarrows 2H^+ + NO_3^- + NO_2^- \quad (8)$$

$$NO_2^- + H_2O \rightarrow 2H^+ + NO_3^- + 2e^- \quad (9)$$

$$[GO\text{–}Fe^{3+}/Fe^{3+}]_{film} + e^- \rightarrow [GO\text{–}Fe^{3+}/Fe^{2+}]_{film} \quad (10)$$

The Fe^{2+}/Fe^{3+} catalyst in GO–PB nanocomposite is electrochemically oxidised to Fe^{3+}/Fe^{3+} (eqn (6)). The catalyst formed adduct with NO_2^- molecules while the NO_2^- ions are oxidised to NO_2 intermediates (eqn (7)). Further oxidation of NO_2 intermediates gives nitrate (NO_3^-) (eqn (8) and (9)) and the PB catalyst was simultaneously regenerated on the electrode (eqn (10)).

4. Conclusions

The study described successful modification of Pt electrode with GO–Fe_2O_3 and GO–PB nanocomposite. Pt–GO–Fe_2O_3 and Pt–GO–PB nanocomposite electrodes were found to have better electron transport and higher nitrite and nitric oxide oxidation current compared to the bare Pt and other electrodes investigated. Electrocatalytic oxidation of the analytes on Pt–GO–Fe_2O_3 and Pt–GO–PB electrodes was diffusion controlled but characterised with some adsorption of electro-oxidation reaction intermediates products. Pt–GO–Fe_2O_3 gave best performance towards electrocatalytic oxidation of NO_2^- and NO in terms of (i) current recovery after multiple runs in the analytes, (ii) resistance to electrode poisoning, (iii) catalytic rate constant and (iv) lower limit of detection. After electrochemical cleaning and reuse, both the GO–Fe_2O_3 and GO–PB nanocomposite modified electrodes gave nitrite and nitric oxide recovery current of about 85–90% indicating a physical adsorption (physisorption) process. Despite the electrodes kinetic limitation due to adsorption, their detection limit, sensitivity and catalytic rate constant values agreed favourably with values previously reported in literature. Interference studies are also reported.

Acknowledgements

The Material Science Innovation & Modelling (MaSIM) Research Focus Area, Faculty of Agriculture, Science and Technology, North-West University (Mafikeng Campus) and the Sasol Inzalo/National Research Foundation (NRF) Innovative bursary supported this project. ASA thanks the North-West University for post-doctoral fellowship and Obafemi Awolowo University Nigeria for the research leave visit. EEE acknowledges National Research Foundation (NRF) of South Africa for incentive funding.

References

1 R. J. Aitken, M. Q. Chaudhry, A. B. A. Boxall and M. Hull, *Occup. Med.*, 2006, **56**, 300.
2 B. Nowack and T. D. Bucheli, *Environ. Pollut.*, 2007, **150**, 5.
3 A. Balamurugan, G. Sockalingum, J. Michel, J. Faure, V. Banchet, L. Wortham, S. Bouthors, D. Laurent-Maquin and G. Balossier, *Mater. Lett.*, 2006, **60**, 3752.
4 A. S. Adekunle and K. I. Ozoemena, *Int. J. Electrochem. Sci.*, 2010, **5**, 1726.
5 A. S. Adekunle, B. O. Agboola, J. Pillay and K. I. Ozoemena, *Sens. Actuators, B*, 2010, **148**, 93.
6 N. Laosiripojana, W. Sutthisripok and S. Assabumrungrat, *Chem. Eng. J.*, 2005, **112**, 13.
7 S. Radhakrishnan, K. Krishnamoorthy, C. Sekar, J. Wilson and S. J. Kim, *Appl. Catal., B*, 2014, **22**, 148.
8 S. Wang, Q. Xu, X. Zhang and G. Liu, *Electrochem. Commun.*, 2008, **10**, 411.
9 R. M. Cornell and U. Schwertmann, *The Iron Oxides: Structure, Properties, Reactions, Occurrences and Uses*, Wiley-VCH, Weinheim, 2nd edn, 2003.
10 G. Selvarani, S. K. Prashant, A. K. Sahu, P. Sridhar, S. Pitchumani and A. K. Shukla, *J. Power Sources*, 2008, **17**, 86.
11 K. C. Pan, C. S. Chuang, S. H. Cheng and Y. O. Su, *J. Electroanal. Chem.*, 2001, **501**, 160.
12 D. Moscone, D. D'Ottavi, D. Compagnone, G. Palleschi and A. Amine, *Anal. Chem.*, 2001, **73**, 2529.
13 A. K. Gein, *Science*, 2009, **324**, 1526.
14 P. V. Kamat, *J. Phys. Chem. Lett.*, 2011, **2**, 242.
15 C. N. R. Rao, A. K. Sood, R. Voggu and K. S. Subrahmanyam, *J. Phys. Chem. Lett.*, 2010, **1**, 572.
16 M. H. Liang, B. Luo and L. J. Zhi, *Int. J. Energy Res.*, 2009, **33**, 1161.
17 P. V. Kamat, *J. Phys. Chem. Lett.*, 2010, **1**, 520.
18 W. S. Hummers and R. E. Offerman, *J. Am. Chem. Soc.*, 1958, **80**, 1339.
19 N. A. Ketov, *Nature*, 2006, **442**, 254.
20 H. He, J. Klinowski and M. Forster, *Chem. Phys. Lett.*, 1998, **287**, 53.
21 F. Uhl and C. Wilkie, *Polym. Degrad. Stab.*, 2004, **84**, 215.
22 R. N. Goyal, A. K. Pandey, D. Kaur and A. Kumar, *J. Nanosci. Nanotechnol.*, 2009, **9**, 4692.
23 T. Maiyalagan, J. Sundaramurthy, P. S. Kumar, P. Kannan, M. Opallo and S. Ramakrishna, *Analyst*, 2013, **138**, 1779.
24 M.-Y. Wang, T. Shen, M. Wang, D.-E. Zhang and Z.-wei Tong, *Sens. Actuators, B*, 2014, **190**, 645.
25 M. Abaker, A. Umar, S. Baskoutas, G. N. Dar, S. A. Zaidi, S. A. Al-Sayari, A. Al-Hajry, S. H. Kim and S. W. Hwang, *J. Phys. D: Appl. Phys.*, 2011, **44**, 5401.

26 Y. Zhang, X. M. Sun, L. Z. Zhu, H. B. Shen and N. Q. Jia, Electrochemical sensing based on graphene oxide/Prussian blue hybrid film modified electrode, *Electrochim. Acta*, 2011, **56**, 1239.
27 A. M. Vinu Mohan, K. K. Aswini, A. Maria Starvin and V. M. Biju, *Anal. Methods*, 2013, **5**, 1764.
28 L. Gao, J. He, W. Xu, J. Zhang, J. Hui, Y. Guo, W. Li and C. Yu, *Biosens. Bioelectron.*, 2014, **62**, 79.
29 A. S. Adekunle, J. Pillay and K. I. Ozoemena, *Electrochim. Acta*, 2010, **55**, 4319.
30 D. Ning, H. Zhang and J. Zheng, *J. Electroanal. Chem.*, 2014, **717**, 29.
31 A. S. Adekunle, B. B. Mamba, B. O. Agboola and K. I. Ozoemena, *Int. J. Electrochem. Sci.*, 2011, **6**, 4388.
32 C. AitRamdane-Terbouche, A. Terbouche, S. Djebbar and D. Hauchard, *Talanta*, 2014, **119**, 214.
33 G. O. Ogunlusi, A. S. Adekunle, N. W. Maxakato and B. B. Mamba, *Int. J. Electrochem. Sci.*, 2012, **7**, 2904.
34 Y. Sahraoui, S. Chaliaa, A. Maaref, A. Haddad and N. Jaffrezic-Renault, *J. Sens. Technol.*, 2013, **3**, 84.
35 A. Rahim, L. S. S. Santos, S. B. A. Barros, L. T. Kubota, R. Landers and Y. Gushikem, *Electroanalysis*, 2014, **26**, 541.
36 K. Zhao, H. Song, S. Zhuang, L. Dai, P. He and Y. Fang, *Electrochem. Commun.*, 2007, **9**, 65.
37 A. S. Adekunle, J. A. O. Oyekunle, O. S. Oluwafemi, A. O. Joshua, W. O. Makinde, A. O. Ogunfowokan, M. A. Eleruja and E. E. Ebenso, *Int. J. Electrochem. Sci.*, 2014, **9**, 3008.
38 R. Ojani, J.-B. Raoof and V. Rahemi, *J. Chin. Chem. Soc.*, 2011, **58**, 247.
39 J. Davis and R. G. Compton, *Anal. Chim. Acta*, 2000, **404**, 241.
40 J. S. Beckman, J. Chen, H. Ischiropoulos and J. P. Crow, *Methods Enzymol.*, 1994, **233**, 229.
41 P. C. Ford, *Pure Appl. Chem.*, 2004, **76**, 335.
42 A. Denicola, J. M. Souza, R. Radi and E. Lissi, *Arch. Biochem. Biophys.*, 1996, **328**, 208.
43 N. Pourreza, M. Fat'hi and A. Hatami, *Microchem. J.*, 2012, **104**, 22.
44 V. Vishnuvardhan, R. Kala and T. P. Rao, *Anal. Chim. Acta*, 2008, **623**, 53.
45 I. M. P. L. V. O. Ferreira and S. Silva, *Talanta*, 2008, **74**, 1598.
46 X. Wang, E. Adams and A. Van Schepdael, *Talanta*, 2012, **97**, 142.
47 A. Kazemzadeh and A. Ensafi, *Anal. Chim. Acta*, 2001, **442**, 319.
48 K. Zhang, L. L. Zhang, X. S. Zhao and J. Wu, *Chem. Mater.*, 2010, **22**, 1392.
49 L. Shahriary and A. A. Athawale, *International Journal of Renewable Energy and Environmental Engineering*, 2014, **2**, 58.
50 H. Guo, X. Wang, Q. Qian, F. Wang and X. Xia, *ACS Nano*, 2009, **3**, 2653.
51 S. Reich and C. Thomsen, *Philos. Trans. R. Soc., A*, 2004, **362**, 2271.
52 Y. Wang, D. C. Alsmeyer and R. L. McCreery, *Chem. Mater.*, 1990, **2**, 557.
53 K. N. Kudin, B. Ozbas, H. C. Schniepp, R. K. Prud'homme, I. A. Aksay and R. Car, *Nano Lett.*, 2008, **8**, 36.
54 K. Ai, Y. Liu, L. Lu, X. Cheng and L. Huo, *J. Mater. Chem.*, 2011, **21**, 3365.
55 A. Kaniyoor and S. Ramaprabhu, *AIP Adv.*, 2012, **2**, 2183.
56 A. M. Farah, N. D. Shooto, F. T. Thema, J. S. Modise and D. D. E. D. Ezekiel, *Int. J. Electrochem. Sci.*, 2012, **7**, 4302.
57 S. Xu, L. Yong and P. Wu, *ACS Appl. Mater. Interfaces*, 2013, **5**, 654.
58 F. T. Thema, M. J. Moloto, E. D. Dikio, N. N. Nyangiwe, L. Kotsedi, M. Maaza and M. Khenfouch, *J. Chem.*, 2013, DOI: 10.1155/2013/150536.
59 Y.-K. Sun, M. Ma, Y. Zhang and N. Gu, *Colloids Surf., A*, 2004, **245**, 15.
60 N. Kijima, M. Yoshinag, J. Awaka and J. Akimoto, *Solid State Ionics*, 2011, **192**, 293.
61 Y.-L. Hu, J.-H. Yuan, W. Chen, K. Wang and X.-H. Xia, *Electrochem. Commun.*, 2005, **7**, 1252.
62 A. Ernst, O. Makowski, B. Kowalewska, K. Miecznikowski and P. J. Kulesza, *Bioelectrochemistry*, 2007, **71**, 23.
63 C. Yang, Q. Lu and S. Hu, *Electroanalysis*, 2006, **18**, 2188.
64 D. Zheng, C. Hu, Y. Peng and S. Hu, *Electrochim. Acta*, 2009, **54**, 4910.
65 W. J. R. Santos, P. R. Lima, A. A. Tanaka, S. M. C. N. Tanaka and L. T. Kubota, *Food Chem.*, 2009, **113**, 1206.
66 P. Wang, Z. Mai, Z. Dai, Y. Li and X. Zou, *Biosens. Bioelectron.*, 2009, **24**, 3242.
67 Y. Cui, C. Yang, W. Zeng, M. Oyama, W. Pu and J. Zhang, *Anal. Sci.*, 2007, **23**, 1421.
68 M. Badea, A. Amine, G. Palleschi, D. Moscone, G. Volpe and A. Curulli, *J. Electroanal. Chem.*, 2001, **509**, 66.
69 *User Manual for Frequency Response Analysis (FRA) for Windows version 4.9*, Eco Chemie B.V., Utrecht, The Netherlands, 200, and references therein.
70 B. A. Boukamp, *J. Electrochem. Soc.*, 1995, **142**, 1885.
71 G. Nurk, H. Kasuk, K. Lust, A. Janes and E. Lust, *J. Electroanal. Chem.*, 2003, **553**, 1.
72 Z. Xu, N. Gao, H. Chen and S. Dong, *Langmuir*, 2005, **21**, 10808.
73 A. J. Bard and L. R. Faulkner, *Electrochemical Methods: Fundamentals and Applications*, John Wiley & Sons, Hoboken, NJ, 2nd edn, 2001.
74 J. N. Soderberg, A. C. Co, A. H. C. Sirk and V. I. Birss, *J. Phys. Chem. B*, 2006, **110**, 10401.
75 G. D. Christian, *Analytical Chemistry*, Wiley, New York, 6th edn, 2004, p. 113.
76 H. X. Ju and L. Donal, *J. Electroanal. Chem.*, 2000, **484**, 150.
77 F. Armijo, M. C. Goya, M. Reina, M. J. Canales, M. C. Arevalo and M. J. Aguire, *J. Mol. Catal. A: Chem.*, 2007, **268**, 148.

